Jpn. J. Appl. Phys. Vol. 42 (2003) pp. 1609–1613
Part 1, No. 4A, April 2003

Propagation of Focused Terahertz Pulses through Subcentimeter Conductive Apertures

Keiji TUKAMOTO*, Rakchanok RUNGSAWANG and Toshiaki HATTORI†

Institute of Applied Physics, University of Tsukuba, 1-1-1 Tennodai, Tsukuba, Ibaraki 305-8573, Japan

(Received July 25, 2002; accepted for publication November 13, 2002)

Temporal waveforms of focused terahertz (THz) pulses, generated from a large-aperture photoconductive antenna, which were passed through conductive apertures were studied. The observed terahertz waveforms formed a large negative tail following the main peak, which was dependent on the aperture size. The observed features were reproduced by simulation using an analytic waveguide model which assumes a single cutoff frequency for the conductive aperture. This feature was observed using conductive apertures of subcentimeter (about 1 to 9 mm) diameter and thickness. Distortion of THz waveforms can be caused when using typical optics such as metal crystal holders that are unintentionally put in the path of THz propagation. Approximately half-cycle pulses without tails were generated by carefully avoiding this effect.
[DOI: 10.1143/JJAP.42.1609]

KEYWORDS: terahertz, femtosecond, half-cycle pulse, large-aperture photoconductive antenna, waveguide effect

1. Introduction

Generation techniques of terahertz (THz) electromagnetic pulses that are based on the use of femtosecond optical pulses have become widely used and have made studies on using THz radiation increasingly important for various applications. One particular antenna structure which generates a very high THz field is the large-aperture biased photoconductive antenna. In addition to the generation of a high THz field, another feature of focused THz pulses generated by this method is the characteristic spectrum which extends from dc to above 3 THz, with a peak at a relatively low frequency. In the time domain, the temporal waveforms can be nearly half-cycle.[1)] Since the generated THz pulse has a large portion of low-frequency components with wavelengths which are large compared with the size of normal optics, THz pulses can undergo drastic changes in temporal and spatial waveforms during propagation through free space or normal optics. In the previous paper, we studied the temporal waveform change of THz pulses near the beam focus and we simulated the observed waveforms using the Gaussian beam model.[2)] We also conducted a time-domain knife-edge measurement of a focused high-peak-field THz beam to confirm the frequency-dependent focusing of THz pulses.[3)] The phenomena observed in these studies are caused by the broad nature of the spectrum of THz pulses.

Various studies based on time-domain spectroscopy[4)] of THz pulses involved only the change in the complex spectral amplitude of THz radiation and did not explicitly require complete information on the temporal waveforms. Therefore, the behavior of temporal THz waveforms has not been yet extensively studied or observed. Understanding the waveform of THz pulses in the time domain should provide insight into its generation process and provide a path to the research of nonlinear material responses to THz pulses. The broad spectrum of a half-cycle THz pulse, as well as the unipolar shape of its electromagnetic field, is expected to have a variety of applications if it can be experimentally properly realized. However, experimental results observed by many groups using similar setups[1,5,6)] show a nearly half-cycle peak with an additional negative tail following the main peak. Observation of a completely half-cycle THz pulse requires the features of generation and propagation to be precisely tailored in the experimental setup.

Propagation through conductive apertures can be used to intentionally change the temporal shape of THz pulses. Temporal and spatial shaping of THz pulses using conductive apertures have been reported by Bromage *et al.*[7)] They effectively used the features of submillimeter conductive apertures for passive spatiotemporal shaping of THz pulses. The apertures used in their study were slits formed with two edges of metal plates, with typical slit widths of 0.1 to 5.0 mm and thicknesses of 0.1 and 1.7 mm. The propagated waveforms were also numerically simulated by the finite-difference time domain (FDTD) method, and an analytical waveguide model was used to explain the observed features. Gallot *et al.* demonstrated coupling of THz pulses to THz waveguides[8)] with typical waveguide cross-sectional dimensions on the order of 300 μm and guide lengths of 25 mm. They comprehensively studied and achieved single-mode propagation of THz pulses with ultrawide pulse bandwidths. The coupling coefficients for the THz beam input to the waveguide modes were calculated. It was shown that linearly polarized input THz pulses are significantly coupled to only a few low-order modes of the specific waveguides.

In contrast to the preceding studies, in this study, we studied propagation through conductive apertures of subcentimeter size and thickness. A typical crystal sample holder made of metal would have a window size and thickness of these dimensions, which might be unintentionally used in THz experimental setups. Aperture dimensions of this size can significantly effect the THz pulse because of the large portion of low-frequency components in the THz pulse. In this study, a conductive waveguide model was constructed to simulate the propagated waveforms. The features in the experimentally observed waveforms were reproduced in simulations using this model. Experimentally, almost half-cycle pulses were generated by carefully avoiding the waveguide effect.

2. Experiments and Results

Temporal field waveforms of focused THz pulses were observed by the electrooptic (EO) sampling method[9)] with the experimental setup shown in Fig. 1. In our experiment, THz pulses were generated by a large-aperture photocon-

*E-mail address: tukamoto@laserlab.bk.tsukuba.ac.jp
†E-mail address: hattori@bk.tsukuba.ac.jp

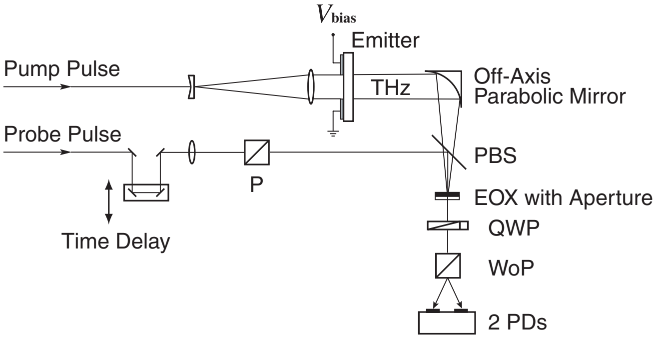

Fig. 1. Schematic of the experimental setup. P: polarizer, PBS: pellicle beamsplitter, EOX: EO crystal (ZnTe), QWP: quarter-wave plate, WoP: Wollaston prism, and PD: photodiode.

ductive antenna. The antenna was constructed by directly placing two aluminum electrodes onto a ⟨100⟩ nondoped semi-insulating GaAs wafer surface with an intergap spacing of 30 mm. The thickness of the GaAs wafer was 350 μm, and the diameter was 50 mm. Pulsed electrical voltage of 12 kV was applied to the electrodes. The width of the voltage pulse was 1 μs and the repetition rate was 1 kHz.

We used a commercially available femtosecond Ti:sapphire regenerative amplifier (Spitfire, Spectra Physics) as the light source for the experiment. The pulse width, center wavelength, and repetition rate of the amplifier output were about 150 fs, 800 nm and, 1 kHz, respectively. The amplified pulses were split into pump and probe beams with pulse energies of 3.8 μJ and about 1 μJ, respectively. The pump beam was expanded and collimated, and was incident on the gap between the electrodes. Spatial distribution of the pump beam on the emitter surface was measured by a knife-edge experiment. It was found to be nearly Gaussian with a 1/e radius of the peak intensity of 9.2 mm. Pump fluence at the center of the emitter was calculated to be 1.4 μJ/cm^2 using these values. THz radiation generated in the transmission direction was focused by a 152-mm-focal-length off-axis parabolic mirror onto a 1.33-mm-thick ⟨110⟩ ZnTe crystal (EO crystal). The probe pulse was loosely focused on the EO crystal and the polarization change induced by the THz field was detected as a function of time delay. A detailed explanation of the EO sampling measurement setup is provided in the previous paper.[1)]

In the experiments, we observed temporal waveform change due to propagation of THz pulses through two types of subcentimeter metal apertures. The first type of metal aperture was one structured in the holder of the EO crystal. This structure was used to hold the EO crystal intact within the holder. There are two pieces to the EO crystal holder (EOXH), the structure of which is depicted in Fig. 2. Both the cover and the engraved piece of bulk that houses the crystal were made of brass. The edge length of the large square face of the 1.33-mm-thick EO crystal was 10 mm. The upper half of the figure shows the front view of the EOXH seen in the direction of the propagation axis of the THz pulse. The lower half shows side views of the EOXH. As shown in the figure, the EO crystal was placed inside an engraved piece of bulk brass that was 10 mm thick. The bulk piece had a square hollow window through which the probe and THz beam passed to reach the EO crystal. The edge

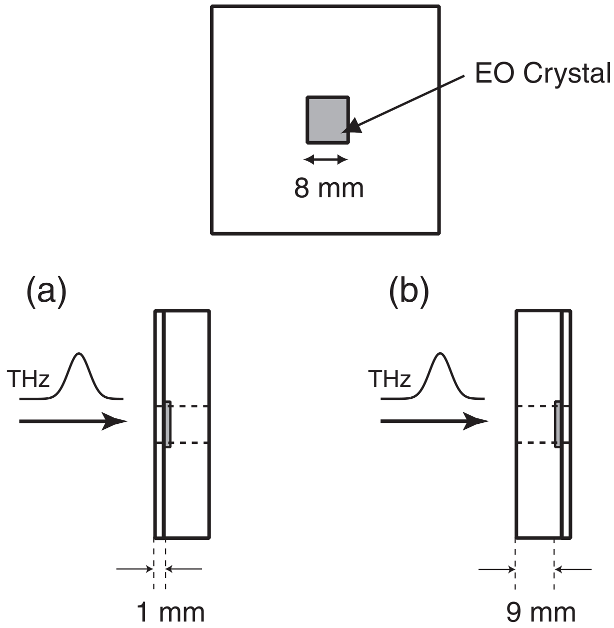

Fig. 2. Diagram of the EO crystal holder (EOXH). The EO crystal is placed inside an engraved piece of bulk brass that is 10 mm thick. Additionally, there is a 1-mm-thick cover that lightly touches the EO crystal. Both the bulk brass and cover have an 8-mm square window in the center through which the probe and the THz beam pass. Upper half: Front view of the EOXH seen in the direction of the propagation of the input THz pulse. Lower half: Side views of the two different orientations for the EOXH with respect to the input THz pulse. The THz pulse propagates through (a) a 1-mm-thick or (b) a 9-mm-thick aperture before reaching the EO crystal.

length of this square window was 8 mm. Additionally, the EO crystal was covered by a 1-mm-thick brass plate that lightly touched the crystal. This cover also had a square hollow window through which the probe beam and THz beam passed. The edge length of this square window was also 8 mm. In the lower figures, (a) and (b) illustrate the two possible orientations of the EOXH with respect to the propagation direction of the input THz pulse. In the experiments, we observed a change in the THz waveform, which is dependent on this propagation direction. In cases of both (a) and (b), the THz pulse must propagate though a square aperture with an edge length of 8 mm. However, there is a difference in the length of propagation through the aperture structure. In case (a), the THz pulse only propagates through a 1-mm-thick square metal aperture before reaching the EO crystal. In contrast, in (b), the THz pulse must propagate through a relatively thick 9 mm aperture before reaching the crystal. We also note that in cases of both (a) and (b), we positioned the EOXH so that the crystal was placed at the focus of the parabolic mirror.

Figure 3 shows the waveforms observed with different orientations of the EOXH. The solid line (a) shows the waveform observed when the THz pulse propagated through the 1-mm-thick square aperture. The dotted line (b) shows the waveform observed when the THz pulse propagated through the 9-mm-thick square aperture. These two waveforms are normalized by their respective peak values. Waveform (b) has a time region in which there is a negative field amplitude following the main peak that persists for about 15 ps before the zero crossing of the THz field. Hereon

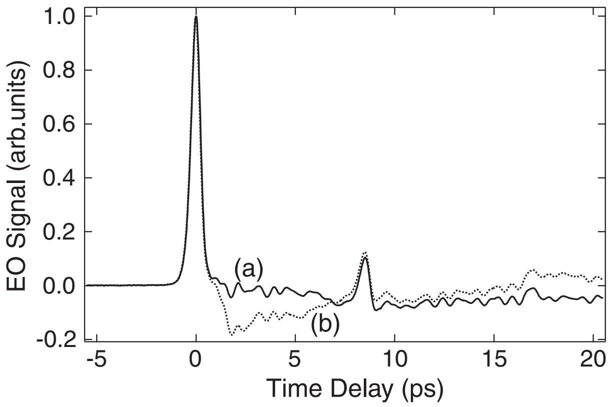

Fig. 3. Experimentally observed field waveforms of focused THz pulses generated from a large-aperture photoconductive antenna. Waveforms (a) and (b) correspond to the EOXH orientations (a) and (b) in Fig. 2, respectively. (a) The waveform observed with a 1-mm-thick square metal aperture in front of the EO crystal. (b) The waveform observed with a 9-mm-thick square metal aperture in front of the EO crystal.

after, we call this part after the main peak the negative tail. Waveform (a), on the other hand, is nearly half-cycle with a very small and slow negative tail with a peak at around 10 ps. We note here that the relatively small peak seen at 8.2 ps is the etalon reflection of the main peak inside the 350-μm GaAs wafer. The small oscillations seen in the waveforms are reproducible, as can be seen by comparing the two waveforms. They are attributed to water vapor absorption.[10)]

We used another type of metal aperture in order to intentionally create the negative tail experimentally. We placed an aluminum plate in front of the EOXH of case (a). The plate was 1.3 mm thick and a circular hole was drilled at the center. We must note that the circular aperture was placed directly in front of the cover of the EOXH, so that the apertures were about 2 mm before the focus. We used two different sizes of circular apertures: apertures with diameters (ϕ) of 3.8 mm and 2.5 mm. The solid lines in Fig. 4 show the THz waveforms observed. The waveform in (a) is the one observed with only a 1-mm-thick square aperture, which was used as a crystal holder cover, as described above, in front of the EO crystal. Waveforms (b) and (c) are those observed with a ϕ 3.8 mm and a ϕ 2.5 mm circular aperture, respectively, in front of the EO crystal in addition to the 1-mm-thick cover. The waveforms in Fig. 4 are all normalized to the peak of waveform (a) and the relative values of the THz field can be compared with each other.

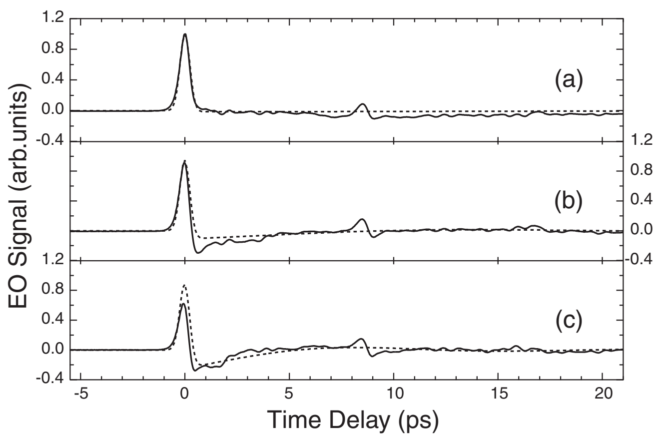

Fig. 4. Waveforms of focused THz pulses that were passed through circular metal apertures of different diameters. Solid lines are the experimental results and the dotted lines are the simulated waveforms. (a) The waveform observed with only a 1-mm-thick square aperture, which was used as a crystal holder cover, in front of the EO crystal. (b) and (c) The waveforms observed with a ϕ 3.8 mm and a ϕ 2.5 mm circular aperture in front of the EO crystal, respectively.

3. Conductive Waveguide Model

In this section, we describe the model used for the simulation of THz waveforms after passing through a metal aperture. A metal aperture acts as a waveguide.[11)] Conductive waveguides have a characteristic cutoff frequency ν_c for each mode that propagates through the structure.[11)] Cutoff frequency ν_c is determined only by the geometrical parameters of the waveguide structure, such as the shape and size, because of the boundary conditions that the fields must hold at the surface walls of the conductive material. Here, we consider square and circular waveguides. Field components below the cutoff frequency cannot propagate through the waveguide while components above can propagate through it. Although each waveguided mode has a different cutoff frequency, we can restrict our consideration to a single cutoff frequency. This is because the coupling of the input field to a single low-order mode is always dominant.[8)] Since the input THz field in our case is nearly linearly polarized, the dominant propagation mode is TE_{10} for a square waveguide, and TE_{11} for a circular waveguide.

The cutoff frequency for the dominant propagation mode TE_{10} for a square waveguide with an edge length of a is given as

$$\nu_c = \frac{c}{2a}, \tag{1}$$

and for mode TE_{11} for a circular waveguide with a radius of r, is given as

$$\nu_c = \frac{1.841}{2\pi} \cdot \frac{c}{r}, \tag{2}$$

where c is the velocity of light in vacuum.[11)]

THz field which propagates through a waveguide can be expressed as

$$E_{wg}(\nu, z) = E_0(\nu) \exp(-i\beta z). \tag{3}$$

Here, $E_0(\nu)$ is the input THz field amplitude of frequency ν, z is the position in the waveguide, and β is the propagation constant. The propagation constant is expressed as a function of frequency as

$$\beta(\nu) = \frac{2\pi}{c}\sqrt{\nu^2 - \nu_c^2}. \tag{4}$$

Below the cutoff frequency ν_c, the field is evanescent and decays exponentially as

$$E_{wg}(\nu, z) = E_0(\nu) \exp\left(-\frac{2\pi z}{c}\sqrt{\nu_c^2 - \nu^2}\right). \tag{5}$$

Above the cutoff frequency ν_c, the field only changes its phase as

$$E_{wg}(\nu, z) = E_0(\nu) \exp\left(-i\frac{2\pi z}{c}\sqrt{\nu^2 - \nu_c^2}\right). \tag{6}$$

In the simulations, we assumed that coupling between the input field to the waveguided mode and between the waveguided mode to the output field is unity. Since in the present study, the input THz field is focused, the couplings should be high and frequency independent in the high-frequency region, whereas in the low-frequency region where the beam waist becomes larger than the aperture size, the coupling should become lower. However, the simulation results obtained without this frequency-dependent coupling reproduced fairly well the behaviors revealed by the experimental results, as described below. Detailed discussion of the effect of this spatial filtering will be given in the next section. We assumed a temporal waveform of the input THz pulse to be Gaussian as

$$E_0(t) = E_0 \exp[-t^2/(\delta t)^2], \tag{7}$$

where E_0 is the field amplitude and $\sqrt{\ln 2}\delta t$ is the full-width at half maximum (FWHM) of the pulse. By defining the geometric size of the waveguide structure and the input THz pulse width δt, we can use the equations shown above to simulate the waveform of a THz pulse that has propagated through a specific square or circular waveguide. In the simulated waveforms below, we assumed an input THz pulse width of 600 fs (FWHM), which is consistent with the experimental results.

Simulated waveforms of THz pulses propagated through a 1-mm- and a 9-mm-thick square conductive waveguide with edge lengths of $a = 8$ mm are shown in Fig. 5. These waveforms are normalized to their respective peaks. The dotted lines in (b) and (c) in Fig. 4 show the simulated waveforms of THz pulses propagated through circular conductive waveguides of ϕ 3.8 mm and 2.5 mm, respectively. The dotted line in (a) shows a simulated waveform without a circular waveguide but with only a 1-mm-thick square conductive waveguide. The thickness of the circular waveguides was set at 1.3 mm in these simulated waveforms.

4. Discussion

The experimental results in Fig. 3 show that the negative tails are observed when the THz pulses propagated through a square metal aperture formed in the EOXH. These waveforms are simulated in Fig. 5 using the simple conductive waveguide model. The dotted waveform (b) in Fig. 5 has a large negative tail that persists for about 12 ps before the zero crossing of the THz field, whereas the solid waveform (a) has a very small negative tail with a long duration. Except for the fact that the etalon reflection peak at 8.2 ps is observed on a negative offset of the THz field, the simulated waveforms in Fig. 5 exhibit the same tendency as the experimental waveforms in Fig. 3. The cutoff frequency for the square conductive waveguide formed in the EOXH is 19 GHz from eq. (1), which corresponds to a cutoff wavelength of 16 mm.

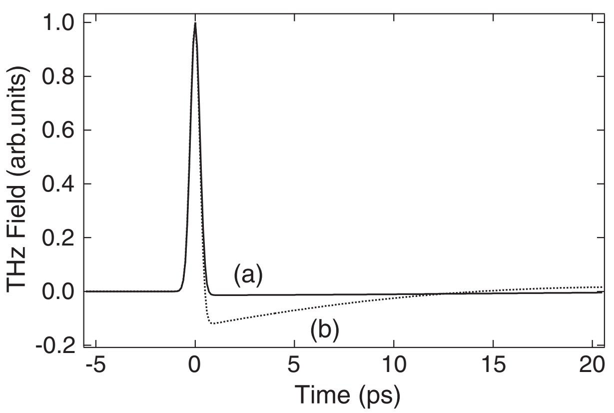

Fig. 5. Simulated waveforms corresponding to the waveforms shown in Fig. 3.

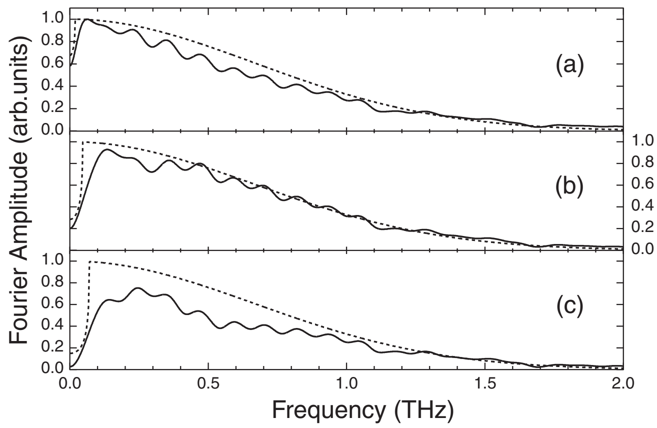

Fig. 6. Fourier amplitude of the waveforms shown in Fig. 4.

The waveform change observed when THz pulses propagated through circular apertures of different diameters, as seen in Fig. 4, shows that when the diameter is smaller, the main peak amplitude becomes smaller and a larger negative tail develops. Fourier amplitudes of the waveforms in Fig. 4 are shown in Fig. 6. Low-frequency components become smaller with smaller diameter, which implies an increase of the cutoff frequency. The cutoff frequencies for the ϕ 3.8 mm and 2.5 mm circular conductive waveguides are 46 GHz and 70 GHz from eq. (2), which correspond to cutoff wavelengths of 6.5 mm and 4.3 mm, respectively.

Since the cutoff effect of the conductive aperture occurs in a relatively low-frequency range, it can be expected that the finite spatial size of focusing optics for the THz beam should also cause a similar negative tail. We have confirmed this by a different calculation as described below. The input THz pulse was assumed to be a Gaussian beam for each frequency component, and the THz beam was focused by an ideal lens which was then passed through a Gaussian aperture.[12] The Gaussian aperture had a spatial transmission profile that is a Gaussian function and was used to model the effect of the finite size of the off-axis parabolic mirror. In this calculation, we found that the focused THz waveform only developed a very small negative tail, which was not consistent with the amplitude of the experimentally observed tail.

A significant difference between the experimental and simulated waveforms is that the amplitude of the negative tail is roughly two times as large for the experimental waveforms compared with the simulated ones. This is probably caused by the simplicity of the theory we applied to simulate these waveforms. Generally, coupling to the waveguided modes is influenced by the polarization, shape, and phase front of the input field. In the simulations, we assumed that coupling between the input field to the waveguided modes was set to a single dominant mode. Also, this coupling is presumed to be independent of frequency. In the actual experimental situation, however, low-frequency components had a beam size larger than the size of the aperture. The experimental results for higher frequency components are rather consistent to the simulated ones, as can be seen in Fig. 6. Therefore, as described below, we can attribute the difference in the amplitude of the low-frequency components between the experimental and simulation results to this frequency-dependent coupling for components with frequency higher than the cutoff frequency but with a beam size larger than that of the aperture.

A focused THz pulse beam has a frequency dependent spatial distribution on the focal plane. We assume here that each frequency component of the THz pulse propagates as a Gaussian beam. Then, the focused beam radius $w_0(\nu)$ for a given frequency ν is $w_0(\nu) = fc/(\pi A \nu)$, where $f = 152$ mm is the focal length of the off-axis parabolic mirror and $A = 9.2$ mm is the beam size of the unfocused THz beam.[2] For the same model, the confocal beam parameter can be expressed as $z_0(\nu) = f w_0(\nu)/A$. In the experiments, we placed the apertures about 2 mm before the focus. This setup should cause the phase front of the field to be nonuniform for higher frequency components. However, since the confocal beam parameter is sufficiently longer than 2 mm for THz frequency less than 2 THz, or in other words, the beam convergence is sufficiently small near the focus, this coupling insufficiency can be neglected. Therefore, the strong suppression of low-frequency components is attributed to the geometrical filtering of low-frequency components of the beam. The beam size of each frequency component of the focused THz beam is inversely proportional to the frequency, as mentioned above. Hence, components with sufficiently low frequencies have a beam size larger than the metal aperture. Thus, the aperture should work as a spatial high-pass filter. This spatial high-pass filtering effect should suppress the coupling of low-frequency components to the aperture waveguide in this setup. This effect should become notable in the frequency region where the beam size becomes comparable to or larger than the size of the aperture. The frequencies that satisfy such a condition for the waveforms seen in Fig. 6 are (a) 0.40 THz, (b) 0.83 THz, and (c) 1.3 THz. A slow decrease of low-frequency components below these frequencies can be observed in the experimental waveforms, whereas the simulated ones have a steep cutoff at a much lower frequency.

Although this incompleteness of the simulations may present a problem in a detailed analysis, the simplicity of the model we constructed here is sufficient to verify that there is a change in the temporal waveform of the scale seen in the experimental results. It is important to note that not only metal crystal holders but also similar conductive structures in the path of THz pulse propagation cause temporal waveform distortion. It should be noted that metal crystal holders are inappropriate for use in THz experiments and special consideration must be made in the selection of optics material to be used in the propagation path of the THz pulse. Equations (5) and (6) show that, for a given aperture size, if the propagation length z satisfies $z \ll c/\nu_c$, the influence on the temporal waveform is negligible. Therefore, the path along which the THz pulse must propagate before reaching the EO crystal should be sufficiently shorter than the cutoff wavelength c/ν_c to not distort the observed waveform.

5. Conclusion

THz pulses generated by a large-aperture photoconductive antenna were focused and passed through square and circular conductive apertures of subcentimeter size and thickness directly before the focus of the THz beam. The observed temporal waveforms formed a negative tail after the main peak. The amplitude of the negative tail was found to increase with smaller aperture size and longer propagation through the aperture. The observed features were reproduced by simulations using a simple conductive waveguide model that assumed a single cutoff frequency for the conductive aperture. By minimizing the waveguiding effect, we have generated nondistorted nearly half-cycle THz pulses.

Acknowledgements

This work was partly supported by the Research Foundation for Opto-Science and Technology, and by the Grant-in-Aid for Scientific Research from the Japan Society for the Promotion of Science.

1) T. Hattori, K. Tukamoto and H. Nakatsuka: Jpn. J. Appl. Phys. **40** (2001) 4907.
2) T. Hattori, R. Rungsawang, K. Ohta and K. Tukamoto: Jpn. J. Appl. Phys. **41** (2002) 5198.
3) K. Tukamoto, R. Rungsawang, T. Fujii and T. Hattori: in preparation for publication.
4) T. D. Dorney, R. G. Baraniuk and D. M. Mittleman: J. Opt. Soc. Am. A **18** (2001) 1562.
5) C. Winnewisser, F. Lewen and H. Helm: Appl. Phys. A **66** (1998) 593.
6) D. J. Cook, J. X. Chen, E. A. Morlino and R. M. Hochstrasser: Chem. Phys. Lett. **309** (1999) 221.
7) J. Bromage, S. Radic, G. P. Agrawal and C. R. Stroud Jr.: J. Opt. Soc. Am. B **15** (1998) 1953.
8) G. Gallot, S. P. Jamison, R. W. McGowan and D. Grischkowsky: J. Opt. Soc. Am. B **17** (2000) 851.
9) Q. Wu and X.-C. Zhang: Appl. Phys. Lett. **67** (1995) 3523.
10) J. Kauppinen, T. Kärkkäinen and E. Kyrö: J. Mol. Spectrosc. **71** (1978) 15.
11) For example; R. E. Collin: *Foundations for Microwave Engineering* (McGraw Hill Kogakusha, Tokyo, 1966).
12) A. E. Siegman: *LASERS* (University Science Books, 1986) p. 786.